RSC Advances

PAPER

View Article Online
View Journal | View Issue

Cite this: *RSC Adv.*, 2019, **9**, 13765

NiO decorated CeO_2 nanostructures as room temperature isopropanol gas sensors†

Nagabandi Jayababu, *[a] Madhukar Poloju, [ab] Julakanti Shruthi [a] and M. V. Ramana Reddy[a]

Heterostructures developed using CeO_2 show promising peculiarities in the field of metal oxide gas sensors due to the great variations in the resistance during the adsorption and desorption processes. NiO decorated CeO_2 nanostructures (NiO/CeO_2) were synthesized *via* a facile two-step process. High resolution transmission electron microscopy (HRTEM) results revealed the perfect decoration of NiO on the CeO_2 surface. The porous nature of the NiO/CeO_2 sensor surface was confirmed from scanning electron microscopy (SEM) analysis. Gas sensing studies of pristine CeO_2 and NiO/CeO_2 sensors were performed under room conditions and enhanced gas sensing properties for the NiO/CeO_2 sensor towards isopropanol were observed. Decoration of NiO on the CeO_2 surface develops a built-in potential at the interface of NiO and CeO_2 which played a vital role in the superior sensing performance of the NiO/CeO_2 sensor. Sharp response and recovery times (15 s/19 s) were observed for the NiO/CeO_2 sensor towards 100 ppm isopropanol at room temperature. Long-term stability of the NiO/CeO_2 sensor was also studied and discussed. From all the results it is concluded that the decoration of NiO on the CeO_2 surface could significantly enhance the sensing performance and it has great advantages in designing best performing isopropanol gas sensors.

Received 17th January 2019
Accepted 29th April 2019

DOI: 10.1039/c9ra00441f

rsc.li/rsc-advances

Introduction

Cerium oxide (CeO_2) is a most abundant rare earth metal oxide in the earth's crust (about 0.0046 wt%) which usually presents in a cubic fluorite structure.[1] The unique properties of CeO_2 like high oxygen storage capacity, existing in two oxidation states (Ce^{4+} and Ce^{3+}), large number of oxygen vacancies, and redox chemistry between Ce^{4+} and Ce^{3+} make it a ubiquitous constituent in various applications.[2,3] The important applications of CeO_2 include solid oxide fuel cells, solar cells, gas sensors, polishing agents, solid electrolytes, catalysts, electrochromic thin films, and energy storage.[4–6] During the past decade, CeO_2 has gradually become a promising metal oxide for gas sensing applications and has gained an upsurge in interest in the field of gas sensors owing to its properties like large number of oxygen vacancies and high oxygen storage capacity.[7] CeO_2 has already proved its ability in detecting various toxic gases like acetone, formaldehyde, ethanol, carbon monoxide, and ammonia.[8–10]

Isopropanol (or isopropyl alcohol) is a colorless and flammable compound with strong odor from the family of volatile organic compounds (VOCs).[11] Isopropanol is being widely used in various applications such as lubricants, solvents, cosmetics, electronic industries for cleaning of printed circuit boards, pharmaceutical industries, household chemicals, and also in automotive field as a petroleum additive.[12–14] However, exposure to isopropanol is very harmful to human health. Dizziness, severe vomiting, irritation of eyes, nose, throat, and mouth are the common symptoms that are being observed while exposing to low concentrated isopropanol (below 400 ppm).[15] Further, exposure to higher concentrations of isopropanol leads to internal bleeding, swelling, excessive sweating, hypertension, breakdown of central nerves system, depression, and coma.[15,16] Therefore, the need of the device which can effectively monitor isopropanol is increasing for environmental control. Some recent studies were succeeded in developing gas sensors using different structured metal oxides to monitor isopropanol efficiently. Xiaoyan cai *et al.* were obtained coral like ZnO–CdO composite with 3D hierarchical porous structure *via* facile self-sustained decomposition of metal–organic compound and tested it for isopropanol sensing performance. The study revealed that the ZnO–CdO composite sensor has shown the highest response and selectivity towards isopropanol at the operating temperature of 248 °C.[17] Bowen Jhang *et al.* developed a sensor using CuO decorated SnO_2 nanorods and showed its best response towards 100 ppm isopropanol at an operating temperature of 280 °C.[18] A recent study of our research group also focused on developing the isopropanol sensor using SnO_2/ZnO core–shell nanostructures and achieved good response at 300 °C operating temperature.[19] Some other researchers also

[a]*Thin Films and Nano Materials Research Laboratory, Department of Physics, Osmania University, Hyderabad-500007, Telangana State, India. E-mail: nagabandi.jay@gmail.com; jaynagabandi@osmania.ac.in; Tel: +91-8978405154*

[b]*Department of Physics, SVS Groups of Institutions, Warangal-506015, TS, India*

† Electronic supplementary information (ESI) available. See DOI: 10.1039/c9ra00441f

tried to fabricate isopropanol sensor and achieved good response at high operating temperatures.[20–22] High operating temperature is the most undesirable quality of any gas sensor which leads to high power consumption, low life time and chance of ignition while dealing with combustible gases.[23]

To get better sensing response at lower operating temperatures, many efforts have been adopted such as, elemental doping, surface modifications, heterostructures, and adding noble metals on the sensor surfaces.[24–28] From past decade heterostructure based hybrid materials are gaining tremendous interest in various fields due to the fact that they can deliver impeccable properties compared to single materials.[29–36] One of the effective methods for the development of sensor which shows high response even at low operating temperature is the formation of heterojunction between CeO_2 and other semiconductor metal oxide. Jie Hu *et al.* synthesized CeO_2 loaded In_2O_3 hollow spheres and obtained enhanced sensing performance towards hydrogen at 160 °C working temperature.[37] Meishan Li *et al.* fabricated a sensor using CeO_2/CdS composites, which shown a significant improvement in the sensing performance towards ethanol at an operating temperature of 161 °C.[38] In particular, the heterostructure formed between CeO_2 and p-type metal oxides is expected to show better sensing performances owing to their great variation at built-in potential near the p–n interfaces. A few recent studies have proved that the coupling of p-NiO with n-type metal oxides could possibly enhances the heterojunction related properties and results in the improved sensing performance.[39,40] However, to the best of our knowledge there are no or less gas sensors which detect isopropanol gas at room temperature.

In this study, NiO decorated CeO_2 nanostructures were prepared and used for gas sensor fabrication. Fabricated NiO/CeO_2 nanocomposite (NC) sensor was investigated for its gas sensing properties towards various toxic gases by measuring the response. The NiO/CeO_2 sensor exhibited better response, sharp response and recovery times, good reproducibility, and long-term stability towards isopropanol at room temperature.

Experimental

Materials

All the chemicals used in this experiment are analytical grade and used as received without further purification. Ammonium ceric nitrate ($(NH_4)_2Ce(NO_3)_6$) with purity of 99% was procured from Himedia and nickel(II) acetate tetrahydrate ($Ni(CH_3CO_2)_2\cdot 4H_2O$) with a purity of 99.9% was obtained from Sigma-Aldrich. 99.9% pure ethanol (C_2H_5OH) was purchased from Himedia to use as solvent. Hydrochloric acid (HCl) with a purity of 35% and monoethanolamine with 99.9% purity were used as stabilizers during the experiment.

Preparation of CeO_2 nanoparticles and NiO decorated CeO_2 nanostructures

CeO_2 nanoparticles (NPs). A typical synthesis of pure CeO_2 NPs using coprecipitation method was as follows: required amount of ammonium ceric nitrate was dissolved in 50 ml distilled water by vigorous stirring on a magnetic stirrer. The clear and transparent solution was obtained after the addition of hydrochloric acid in dropwise manner. This clear and transparent solution was kept on stirring for 1 h at 60 °C and then 10 ml of ammonium hydroxide (NH_4OH) was added to form precipitate. This precipitate was collected and dried at 300 °C for 2 h using an electric bunsen burner to get required CeO_2 nanopowders.

NiO/CeO_2 nanocomposites. Decoration of NiO on CeO_2 nanostructures was a two-step process where CeO_2 precipitate was first collected by using above discussed coprecipitation method. In a separate experiment, 0.2 M nickel acetate tetrahydrate solution was prepared by using nickel(II) acetate tetrahydrate as solute and ethanol as solvent. This solution was stirred by using magnetic stirrer for the complete dissolution of solute in ethanol and then monoethanolamine was added dropwise to get transparent solution. Then first collected CeO_2 precipitate was washed in this nickel contained solution and this washed precipitate was collected using filter paper and dried at 300 °C for 2 h to get required NiO/CeO_2 NC powders.

Fabrication of gas sensors and their gas sensing measurements

The detailed procedure to fabricate the gas sensors and their gas sensing tests are described elsewhere.[19] In brief, thick slurries of both pure CeO_2 NP and NiO/CeO_2 NC powders were prepared separately and coated on alumina plates which are having pre-coated silver electrodes. These coated thick films were dried at a temperature of 80 °C for 3 h on hot plate (Fig. S1†). Custom made gas sensing unit consisting an air sealed glass chamber equipped with a heater, probes, and a thermocouple was utilized to investigate the gas sensing response of the prepared gas sensors (Fig. S2†). Required concentration of the test gas was measured from static liquid distribution method, which was calculated by following equation.

$$C = \frac{22.4 \times \phi \times \rho \times V_1}{M \times V_2} \times 1000 \text{ ppm} \quad (1)$$

where C (ppm) is the required test gas concentration in ppm, ϕ denotes the target gas volume fraction, ρ (g ml^{-1}) indicates the density of the liquid, V_1 (μl) and V_2 (l) are the volumes of liquid and chamber respectively, and M (g ml^{-1}) is the molecular weight of the liquid. The gas sensing response of the sensor was calculated using the following equation

$$S = R_a/R_g \quad (2)$$

where R_a and R_g are the resistances of the sensor in the presence of air and targeted gas respectively. The gas sensing response measuring circuit is schematically presented in Fig. 1. The input voltage of 5 V was supplied to the circuit and output voltage was observed across virtual resistor which varies according to the sensor resistance. The target gas was evaporated by injecting the required amount of liquid onto the hot bottom plate of the chamber. All the gas sensing measurements of the fabricated gas sensors were performed under normal laboratory conditions (~35% RH, 28 °C).

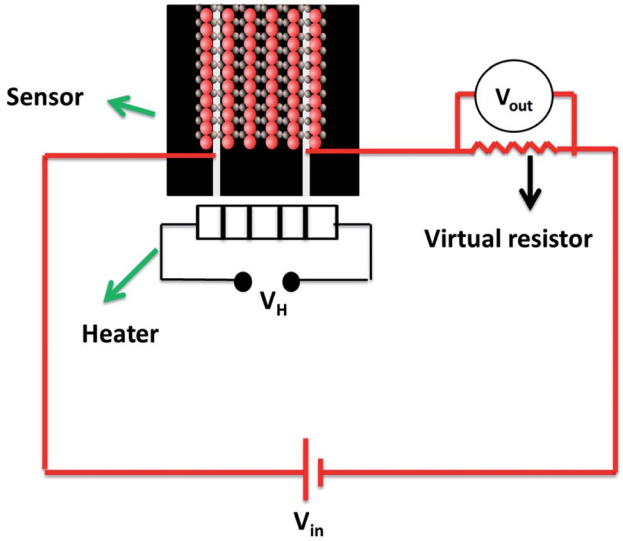

Fig. 1 Schematic representation of gas sensing measurement circuit.

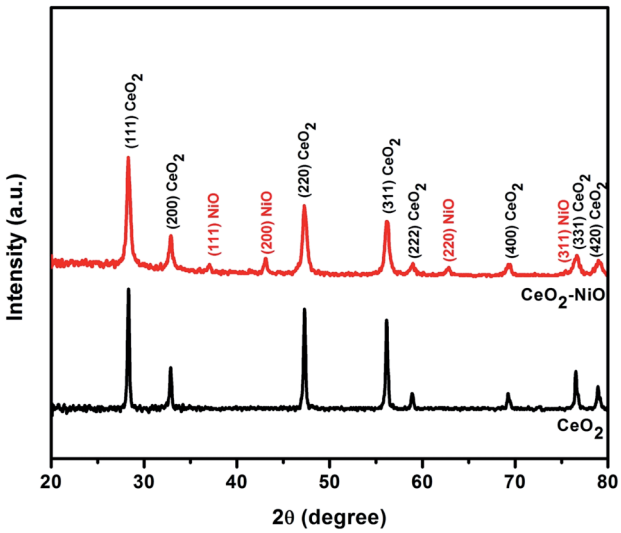

Fig. 2 XRD patterns of pure CeO_2 nanoparticles and NiO/CeO_2 nanocomposites.

Characterization of materials

The phase and crystallinity of the pure CeO_2 NPs and NiO/CeO_2 NCs were examined by powder X-ray diffraction (XRD) patterns recorded on Philips diffractometer (40 kV, 30 mA, Cu K_α radiation with $\lambda = 1.54178$ Å) at room temperature over a 2θ range between 20° to 80°. The surface morphological and chemical compositional studies of the pure CeO_2 NPs and NiO/CeO_2 NCs were carried out by using field emission scanning electron microscopy (FESEM, Zeiss/Ultra 55) equipped with energy dispersive X-ray spectroscope (EDS). After fabricating the gas sensors, the morphology and composition characteristics were analyzed using scanning electron microscope (SEM, Zeiss Evo18) equipped with EDS. X-ray photo electron spectra (XPS) on a PHI5000VersaProbeII system using Al Kα (1486.6 eV) radiation operating at an accelerating power of 15 kW were used to investigate the surface chemical states of the elements in NiO/CeO_2 NCs. The shape, size, and structure related information of NiO/CeO_2 NCs was obtained from high resolution transmission electron microscopy (HRTEM) imaging *via* a JEOL-JEM 2100 system operating at 200 kV.

Results and discussion

Structure and morphology analysis

XRD patterns shown in Fig. 2 were used to investigate the crystalline phases of both pure CeO_2 NPs and NiO/CeO_2 NCs. As observed in the figure, pure CeO_2 is crystallized in face-centered cubic structure with characteristic peaks at $2\theta = 28.32°$, 32.87°, 47.30°, 56.16°, 58.90°, 69.21°, 76.54°, and 78.92° which are corresponding to (111), (200), (220), (311), (222), (400), (331), and (420) planes respectively. All the observed planes are good in accordance with the standard JCPDS file no. 340394. Other diffraction peaks corresponding to any other impurities were not observed which indicates the purity and good crystallinity of the prepared CeO_2 samples. From the XRD patterns of NiO/CeO_2 NCs it is observed that, it has all the peaks corresponding to face centered cubic structure of CeO_2 and in addition, it has diffraction peaks at $2\theta = 37.09°$, 43.11°, 62.87°, and 75.43° which are corresponding to (111), (200), (220), and (311) planes respectively. All these additional peaks are due to the presence of face-centered cubic structure of NiO and are well in accordance with the standard JCPDS card no. 89-7130. It was clearly observed that there were no other peaks related to CeO_2–NiO alloy and no shift in the peaks indicating the perfect formation of NiO/CeO_2 NCs without impurities.

The information related to the valence states of the elements Ce, Ni and O on the surface of the NiO/CeO_2 NCs obtained from XPS and shown in Fig. 3. The XPS survey spectrum presented in Fig. 3(a) shows the signals corresponding to Ce, Ni, O and C which confirms their existence in the sample. Ni 2p XPS spectrum of NiO/CeO_2 NCs is given in Fig. 3(b), which revealed the doublet splitting of 2p into $2p_{3/2}$ and $2p_{1/2}$ states located at 854.33 eV and 872.08 eV respectively along with their respective satellite peaks located at 860.2 eV and 878.45 eV. All these peaks observed are characteristic peaks of Ni^{2+}.[41] XPS spectrum of Ce 3d is a bit complex one due to the presence of several peaks, but the careful evaluation of the peaks will leads to exact estimation of the valence state of Ce. From the Fig. 3(c) there were six peaks presented in the Ce 3d spectrum due to Ce $3d_{3/2}$ and Ce $3d_{5/2}$ at 916.43 eV, 907.06 eV, 900.56 eV, 898.06 eV, 888.43 eV and 882.06 eV which were denoted as U_1, U_2, U_3, V_1, V_2, and V_3 respectively. The peak located at 916.43 eV is the main characteristic peak of Ce^{4+} and the peak at 882.06 eV is the fingerprint peak of CeO_2.[42,43] All the observed peaks are characteristic peaks of Ce^{4+} and well in agreement with the reported results.[44] O 1s XPS profile of NiO/CeO_2 NCs is shown in Fig. 3(d). The peak at 529.06 eV indicates the lattice oxygen in the NiO/CeO_2 NCs ample and the peak at 531.4 eV is due to the physically adsorbed oxygen.[45]

Surface morphological and compositional characteristics of pure CeO_2 NPs and NiO/CeO_2 NCs were investigated by FESEM and EDS respectively (Fig. 4(a–d)). As can be seen from the Fig. 4(a) the pure CeO_2 NPs are in spherical shape with uniform

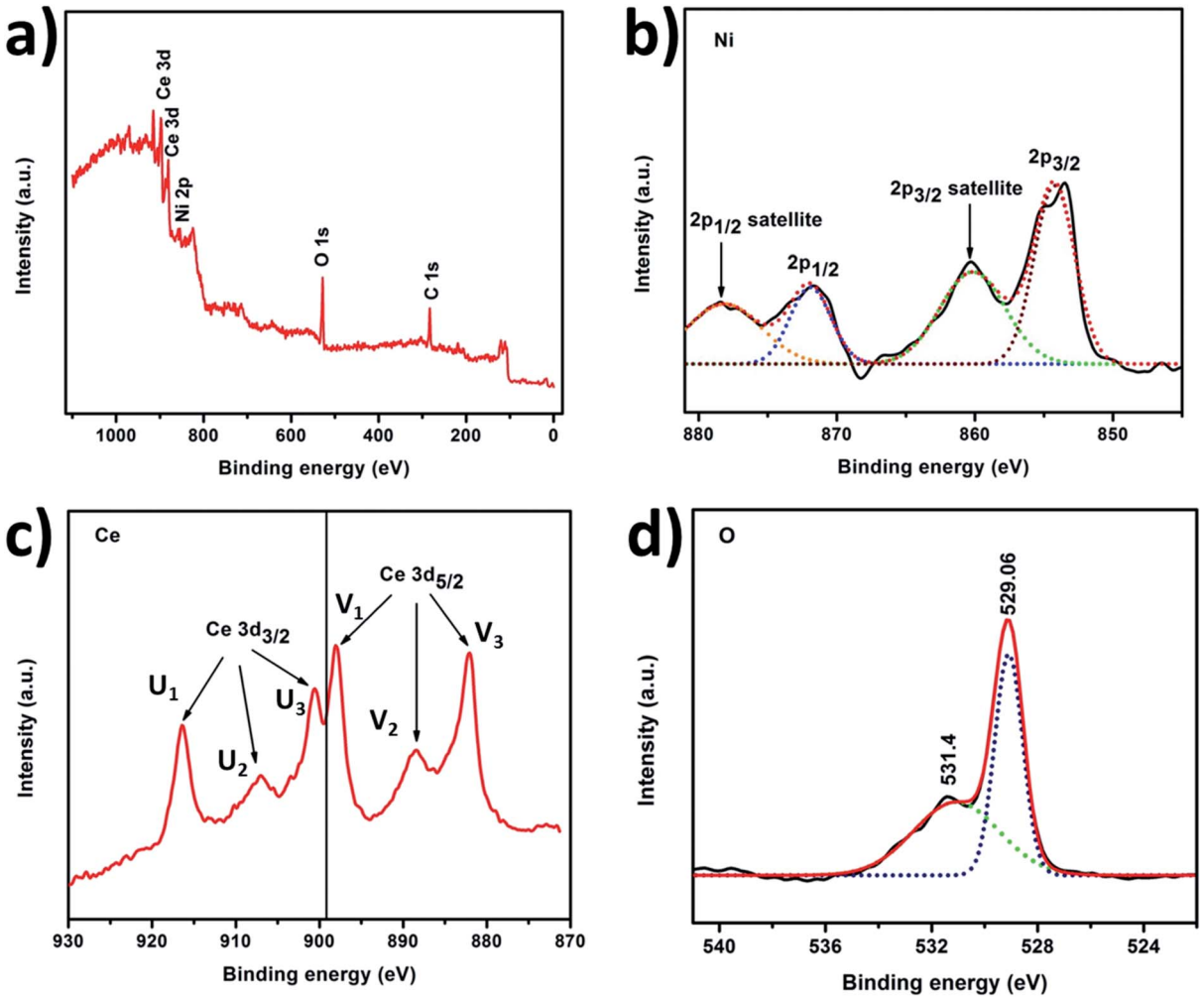

Fig. 3 XPS spectra of (a) NiO/CeO_2, (b) Ni 2p and (c) Ce 3d, and (d) O 1s.

sizes of about 20–35 nm and there are no other morphologies present in the sample indicating the formation of well-defined nanostructures. FESEM image of NiO/CeO_2 NCs shown in Fig. 4(c) demonstrates the regularly shaped grains with sizes around 18–25 nm. The clear identification of NiO decoration on CeO_2 surface is made from HRTEM analysis. From the EDS spectra of pure CeO_2 NPs and NiO/CeO_2 NCs it is obvious that the perfect stoichiometric materials are formed (Fig. 4(a and d)). Surface morphology and elemental analysis of the fabricated gas sensor using NiO/CeO_2 NCs were studied by SEM and EDS respectively and presented in Fig. 4(e and f). As can be observed from the figure the surface of the prepared sensor was highly porous and has good stoichiometry even after the sensor fabrication. Highly surface porous nature of the fabricated sensor will plays a vital role in enhancing the gas sensing properties by facilitating the more surface active sites to adsorb more oxygen species onto the surface.

The morphological characteristics like shape, size, and crystallinity of the NiO/CeO_2 NCs were investigated by HRTEM and shown in Fig. 5(a–d). The decoration of NiO NPs on the surface of CeO_2 was clearly evidenced from the Fig. 5(a and b). As seen from the Fig. 5(a), spherical shaped NiO with an average diameter of about 6 nm was perfectly decorated on ~14 nm sized CeO_2 surface. Further confirmation about decoration was done by calculating *d*-spacing between the planes of NiO/CeO_2 NCs (Fig. 5(c)), as observed from the figure the *d*-spacing of 0.321 nm has been assigned to the (111) plane of CeO_2. The *d*-spacing of 0.199 nm and 0.244 nm was ascribed to (200) and (111) planes of NiO respectively. The selected area electron diffraction (SAED) patterns obtained for NiO/CeO_2 NCs were presented in Fig. 5(d) which shows several diffraction rings. For instance, (200), and (111) are the characteristic planes of CeO_2 in face centered cubic structure and (200), and (111) planes are responsible for decorated NiO which is crystallized in face centered cubic structure. These diffraction results are well in accordance with the XRD results discussed above.

Gas sensing properties

In view of negative effects of isopropanol and its irresistible usage in many applications, the need of an efficient gas sensor which can monitor isopropanol at or near room temperature is increasing in the field of gas sensors. The most promising gas sensors for the monitoring of various gases are mainly

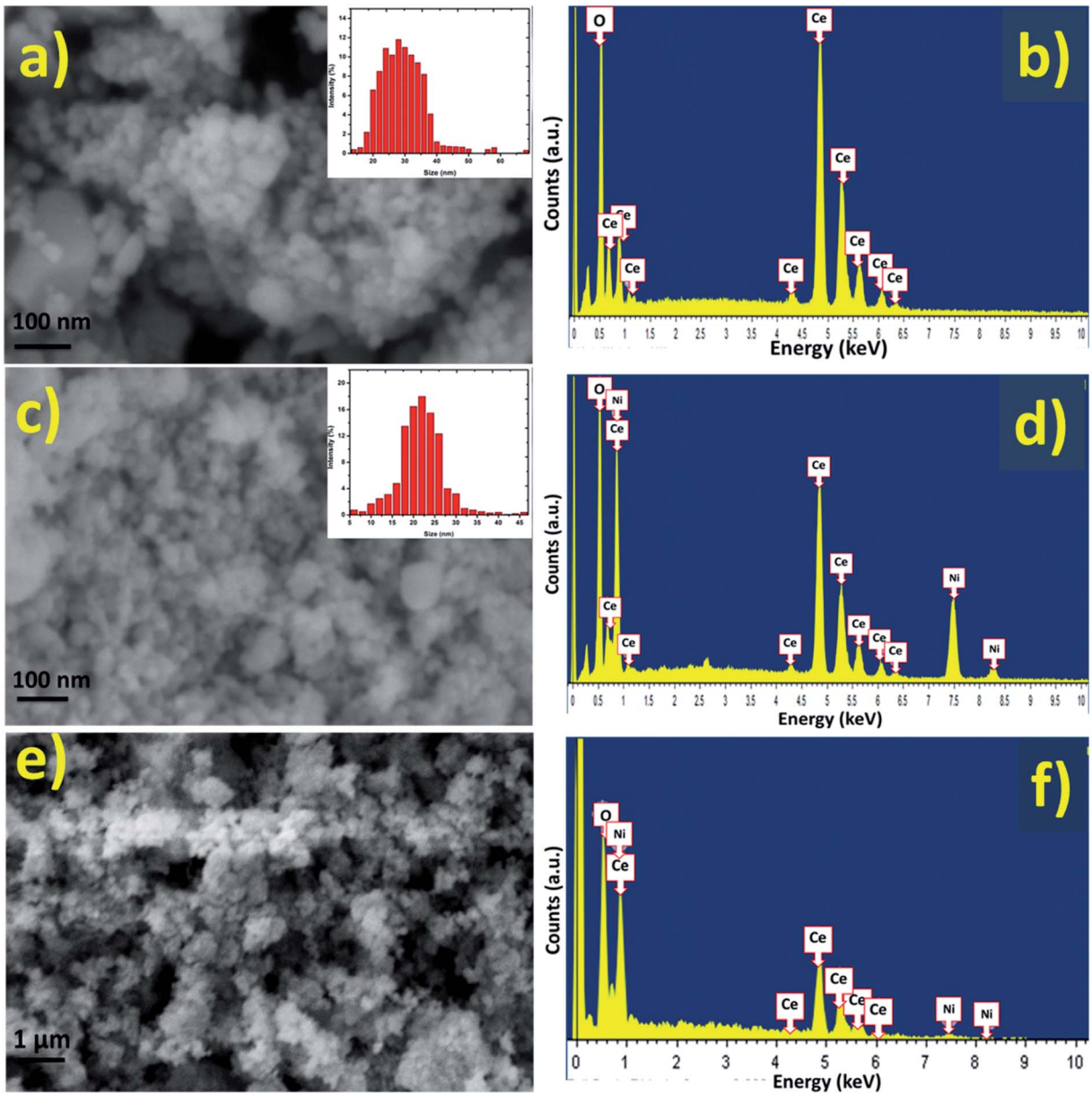

Fig. 4 FESEM images of (a) CeO_2 nanoparticles, (c) NiO/CeO_2 nanocomposites. EDS spectra of (b) pure CeO_2 nanoparticles, and (d) NiO/CeO_2 nanocomposites. (e) SEM micrographs and (f) EDS spectrum of fabricated gas sensor using NiO/CeO_2 nanocomposites. Insets are the particle size distributions.

developed from the various metal oxides. Furthermore, some modifications to the metal oxide based gas sensors like, small grain size and heterojunction formation with porous outer surfaces are helping in significant enhancement in the detection of various gases at or near room temperature. Prepared nanopowders of CeO_2 NPs and NiO/CeO_2 NCs were used to fabricate gas sensors and tested their gas sensing performance at room temperature.

Response and recovery analysis has been adopted for the evaluation of the gas sensing performance of CeO_2 NPs and NiO/CeO_2 NCs based gas sensors towards 100 ppm isopropanol at room temperature and the results are shown in Fig. 6(a and b). From the figure it is noted that the response of the NiO/CeO_2 NCs based gas sensor is much higher than the pure CeO_2 NPs based gas sensor. A highest response of ~1570 was observed for NiO/CeO_2 NCs based gas sensor which is nearly 11 times higher than the pure CeO_2 based gas sensor (~139) towards 100 ppm isopropanol at room temperature. The time taken by the sensor to change 90% of its resistance during the adsorption/desorption process is called as response/recovery time[46] and it is very important parameter in the evaluation of any gas sensor performance. The response and recovery times of CeO_2 NP and NiO/CeO_2 NC based gas sensors also shown in the Fig. 6(a and b). It is noticed that NiO/CeO_2 gas sensor has short response time (15 s) and quick recovery time (19 s) whereas CeO_2 gas sensor has longer response and recovery times (93 s and 117 s respectively) compared to NiO/CeO_2 gas sensor. Heterojunctions formed between n-CeO_2 and p-NiO throughout sensor

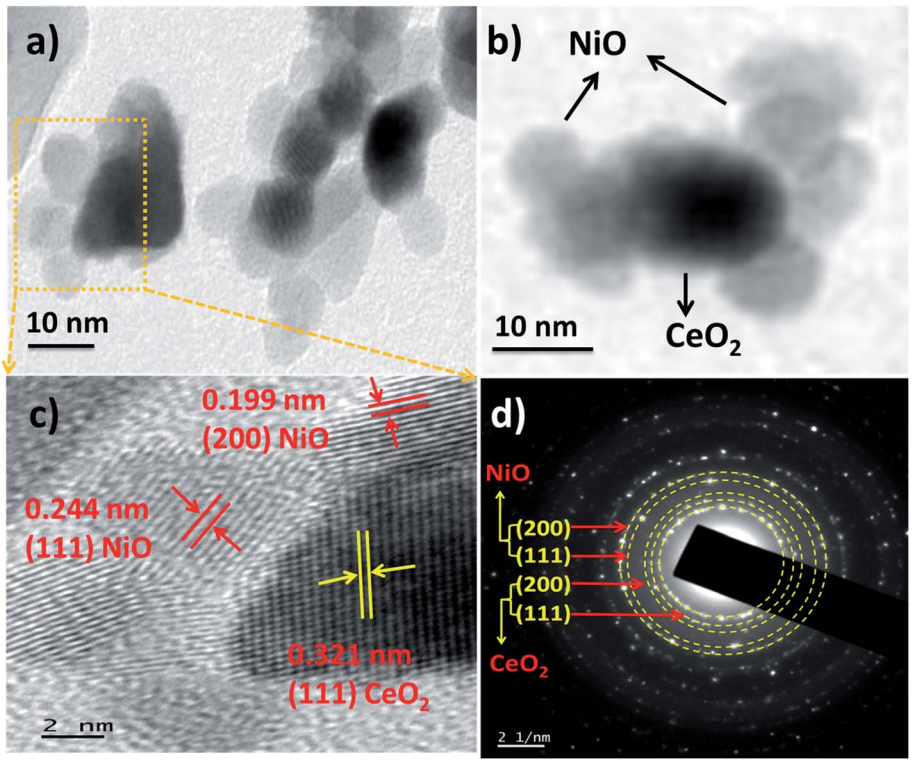

Fig. 5 (a and b) HRTEM images of NiO/CeO_2 nanocomposites with different magnifications. (c) *d*-spacing and (d) SAED pattern of NiO/CeO_2 nanocomposites.

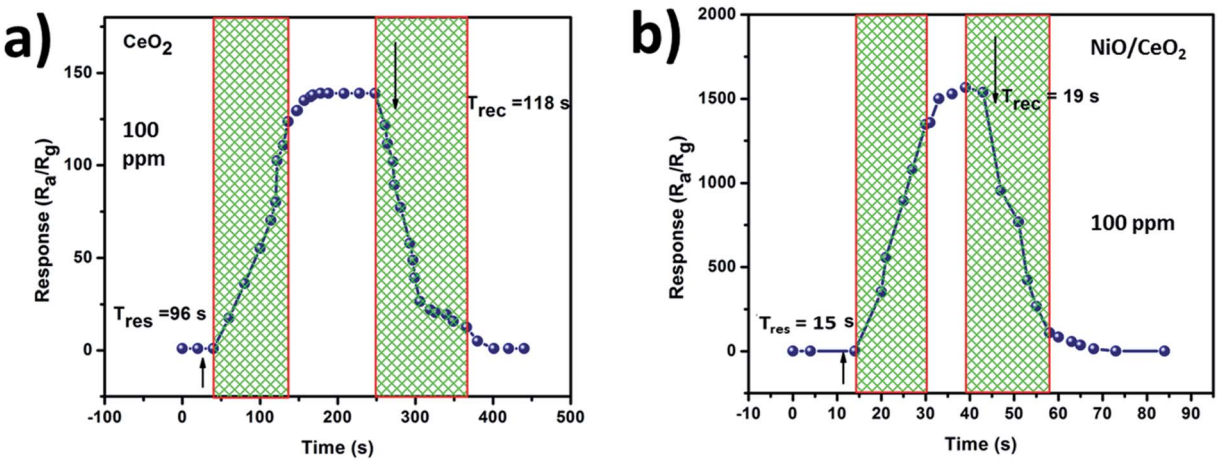

Fig. 6 Response and recovery of (a) CeO_2, and (b) NiO/CeO_2 gas sensors towards 100 ppm isopropanol gas at room temperature.

material are more sensitive to the surrounding atmosphere and pore channels on the outer surface of the sensor could also contributed for the enhanced response of NiO/CeO_2 NCs based gas sensor.

Further, the performance of both the sensors was compared by observing the response of the sensors with respective to the concentration of isopropanol gas (1, 5, 10, 20, 30, 50, 70 and 100 ppm) at room temperature. As shown in Fig. 7(a) the sensor fabricated from NiO/CeO_2 NCs has shown highest response at every concentration of isopropanol compared to pure CeO_2 based gas sensor indicating the better performance of it. A gas sensor which is aimed to use in practical applications must have good response along with better reproducibility. To test its reproducibility, the dynamic response transients of NiO/CeO_2 NCs based gas sensor were recorded at room temperature towards various concentrations of isopropanol gas and shown in Fig. 7(b). As can be seen from the figure the responses of the sensor are 10.83, 75, 131.63, 297.66, 454.41, 731.49, 1122.66, and 1568.16 towards 1, 5, 10, 20, 30, 50, 70 and 100 ppm of isopropanol gas respectively. These results are clearly demonstrating that the response of the sensor towards the isopropanol gas detection is significantly increasing with the concentration

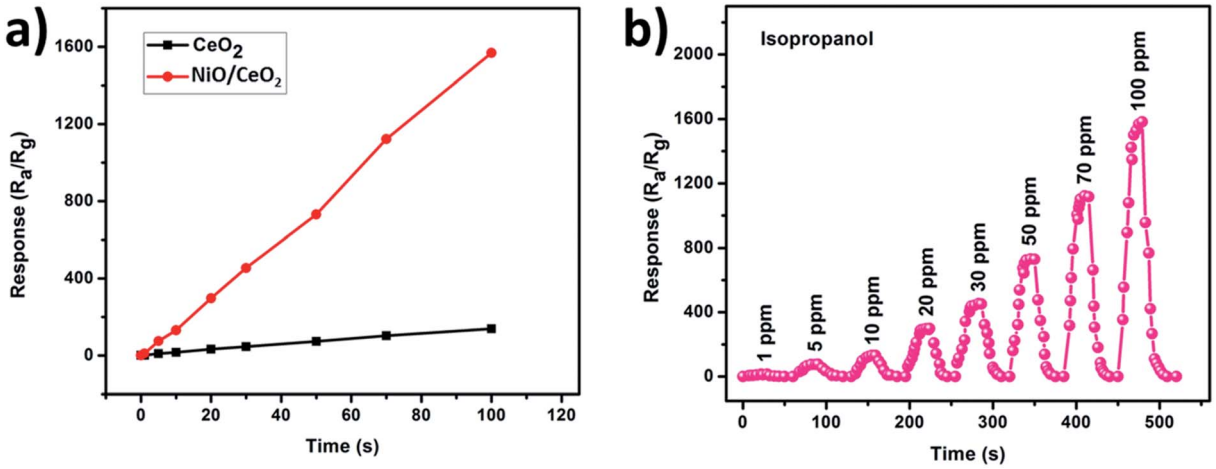

Fig. 7 (a) Response of CeO_2, and NiO/CeO_2 gas sensors towards various concentrations of isopropanol gas at room temperature. (b) Dynamic response and recovery curves of NiO/CeO_2 gas sensor towards isopropanol gas at room temperature.

of the gas which is due to the increasing of gas analytes participating in the adsorption and desorption reactions. A good repeatability during the introduction of test gas as well as fresh air into the chamber also observed from the figure. The NiO/CeO_2 NCs based gas sensor has shown a response of 10.83 towards 1 ppm isopropanol suggesting the good detection ability of sensor even at lower concentrations. Highly porous nature of surface and heterojunctions formed at the two materials interface are responsible for these best gas sensing properties.

Gas sensing response towards various gases like ethanol, 2-methoxyethanol, acetylacetone, *n*-butanol, isopropanol, acetone, xylene, toluene, and methanol was tested for NiO/CeO_2 NCs based gas sensor with varying the concentration of the gases (1, 5, 10, 20, 30, 50, 70 and 100 ppm) at room temperature. As displayed in Fig. 8(a) the sensor response is increasing with the concentration of the gases and shown extremely good response towards isopropanol gas. Further, the response and recovery times towards all the above test gases with 100 ppm concentration were measured at room temperature for both pure CeO_2 and NiO/CeO_2 gas sensors and shown in Fig. 8(b). From the figure it is obviously observed that the NiO/CeO_2 NC gas sensor has shown sharp response and recovery times (15/19 s) towards isopropanol which are very shorter than that of *n*-butanol (67/79 s), ethanol (59/82 s), 2-methoxyethanol (69/92 s), acetylacetone (62/86 s), acetone (51/77 s), xylene (72/80 s), toluene (71/93 s), and methanol (57/69 s).

It is also known that the selectivity of the sensor is a key parameter in estimating the gas sensing performance. Any gas sensor developed to use in practical applications should possess good selectivity towards a particular gas. In general, the ability of the gas sensors in detecting a specific gas among the mixture of several gases is called as selectivity.[47] Selectivities of pure CeO_2 NP and NiO/CeO_2 NC based gas sensors were tested towards nine gases of 100 ppm (2-methoxyethanol, ethanol, acetylacetone, *n*-butanol, isopropanol, acetone, xylene, toluene, and methanol) at room temperature and shown in Fig. 9(a). As displayed in figure, the NiO/CeO_2 NC gas sensor has shown

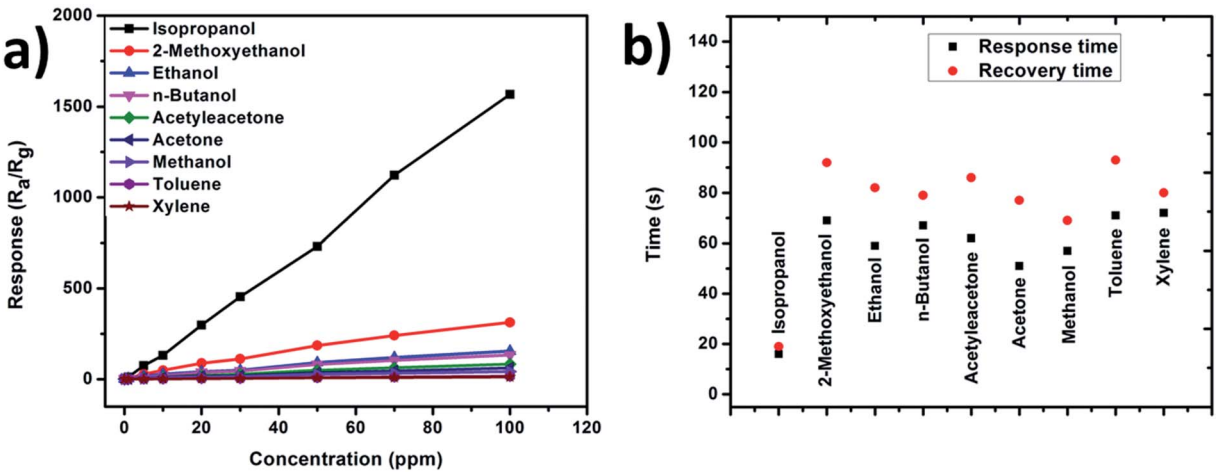

Fig. 8 (a) Response of NiO/CeO_2 gas sensor *versus* varying concentrations (1–100 ppm) of test gases at room temperature. (b) Response and recovery times of NiO/CeO_2 gas sensor towards 100 ppm test gases at room temperature.

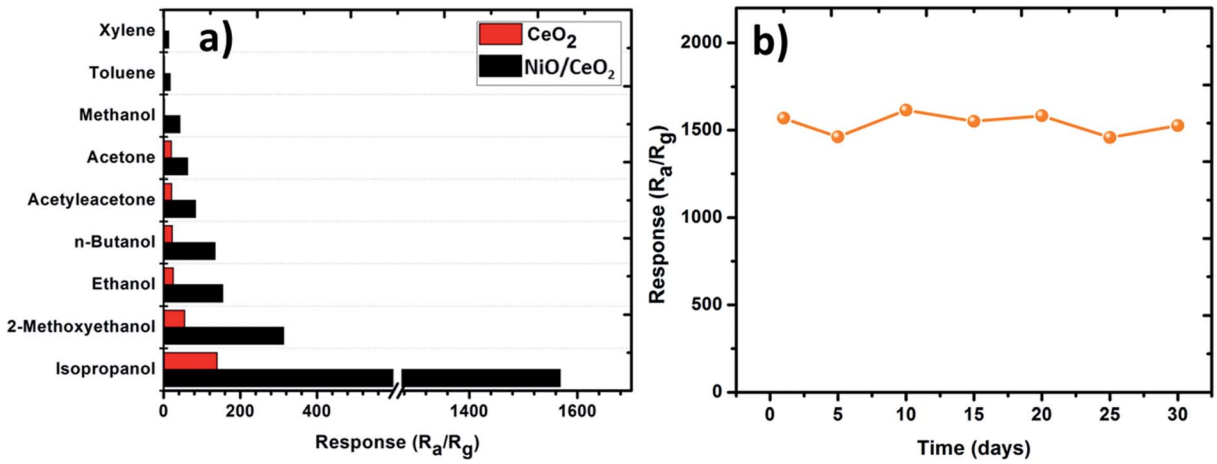

Fig. 9 (a) Response of CeO_2, and NiO/CeO_2 gas sensors towards 100 ppm test gases at room temperature. (b) The long-term stability of NiO/CeO_2 gas sensor towards 100 ppm isopropanol at room temperature.

tremendous response towards isopropanol gas among all the test gases which showing that the sensor has good selectivity towards isopropanol. Different volatilities and different chemical properties of the gases which prompt the sensor to exhibit different adsorption and catalytic performances towards them might be the reason for the different responses.[45]

Long-term stability is another most important characteristic of a practical gas sensor. The stability of NiO/CeO_2 NCs based gas sensor towards 100 ppm of isopropanol was tested at room temperature for 30 days. The obtained stability results are shown in Fig. 9(b) and it is clearly observed that the sensor shows nearly constant response throughout the tested period which indicates its excellent stability. The performance degradation after the first 5 days of fabrication of the sensor is just about 4.75%. Table 1 is the comparison of gas sensing performance of different types of isopropanol gas sensors from the literature.

Isopropanol gas sensing mechanism

CeO_2 gas sensing mechanism can be explained by basic well-known n-type metal oxide sensing mechanism which involves the change of electrical resistance in virtue of adsorption and desorption of oxygen and target gas on the surface of the sensor.[19,48] Fig. 10(b) demonstrates the gas sensing mechanism of CeO_2 sensor. In the presence of air atmosphere, oxygen molecules get adsorbed on the surface of the sensor by extracting the conducting electrons from the sensing material (CeO_2) and form the negatively charged oxygen species ($O_{(ads)}^{2-}$, $O_{2(ads)}^{-}$, $O_{(ads)}^{-}$, and $O_{2(ads)}^{2-}$) which results in the development of electron depletion layer at the air and sensor interface. Extraction of conducting electrons from the sensing material leads to an increase in the resistance of the material. Introduction of any reducing gas (isopropanol in present case) into the sensing chamber results in the release of extracted electrons back to the sensor by getting oxidized into CO_2 and H_2O during which the sensor resistance decreases. This variation of electrical resistance in the presence of air and target gas is the response of the sensor. As the oxygen storage capacity of the CeO_2 is high, it extracts more number of electrons while adsorbing the oxygen and releases maximum electrons while reducing in the presence of reducing gas.

Band diagram of the NiO/CeO_2 NCs before and after junction formation is presented in Fig. 10(a). After decorating NiO NPs on CeO_2 surface, the diffusion of electrons and holes one side to other side takes place until their Fermi levels become equal. Electrons from CeO_2 side diffuse into NiO side and holes from NiO side diffuse into CeO_2 side due to the concentration gradient of the charge carriers. After getting the balanced state of the carriers, Fermi level of the system gets equalized. This whole phenomenon develops an internal potential called built-in potential at the interface of the two materials which further hinders the diffusion of both the charge carriers (electrons and holes). This built-in potential plays a vital role in sensing

Table 1 Comparison of the isopropanol gas sensors from the literature

Material	Isopropanol concentration (ppm)	Operating temperature (°C)	Response (R_a/R_g)	Response/recovery time (s/s)	Ref.
SnO_2 nanorods	2000	325	~125	6/18	22
ZnO–CdO	1000	248	174.8	16/25	17
SnO_2 nanorings	100	250	7.27	6.8/38.6	21
CuO/SnO_2	100	280	50.4	4/9	18
SnO_2/ZnO	500	300	103.3	14/17	19
NiO/CeO_2	100	RT	1568	15/19	This work

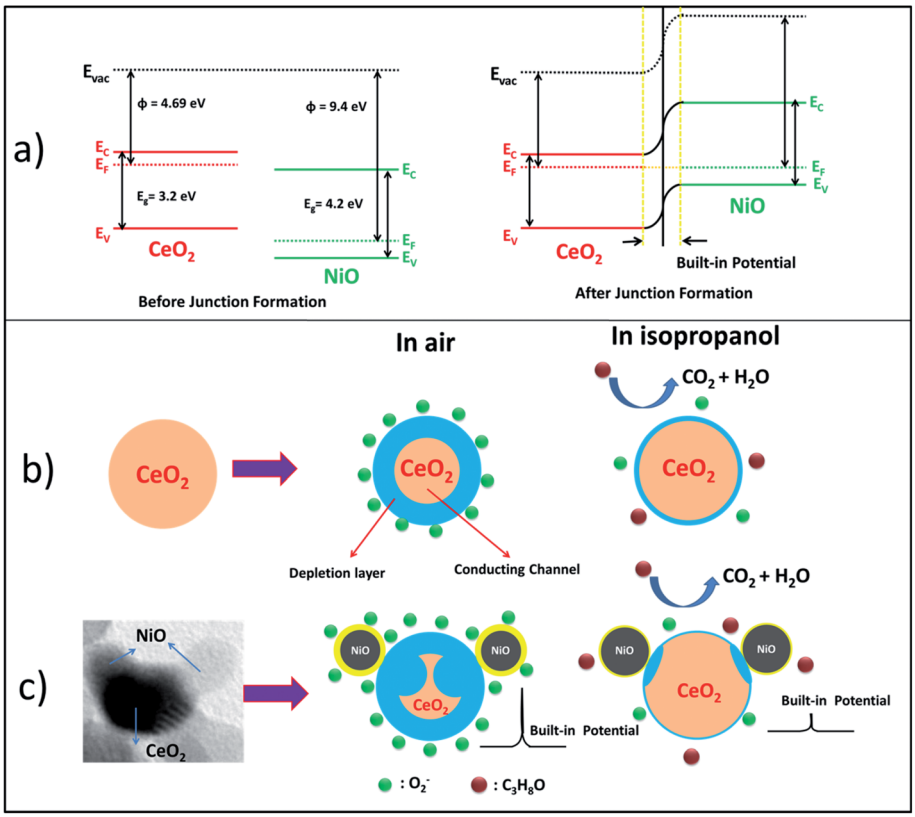

Fig. 10 (a) Schematic diagram demonstrating the band gap alignment of NiO/CeO_2. Schematic illustration of the isopropanol gas sensing mechanism of (b) CeO_2 and (c) NiO/CeO_2 gas sensors with surface adsorption and desorption reactions.

performance of NiO/CeO_2 NCs. In the presence of oxidative and reductive environments the width of the built-in potential varies according to the availability of the charge carriers.

The mechanism involved in the enhanced sensing performance of NiO/CeO_2 NC sensor towards isopropanol at room temperature has been shown in Fig. 10(c). The superior sensing performance of NiO/CeO_2 NCs is presided over by the parameters like, highly porous surface of the sensors, small grain sizes of the sensing material, built-in potential at p-NiO and n-CeO_2 interface, highly catalytic nature and chemical sensitization of decorated NiO, and the behavior of the targeted gas. From the SEM images of the sensors fabricated from NiO/CeO_2 NCs it is clear that the surface of the sensor is highly porous and improves the diffusion rate of air and targeted gas into the sensor. Small grain sizes (<25 nm) as evidenced from the HRTEM studies provide the large active surface area which further helps in enhanced sensing performance.

There are three types of junctions (NiO–NiO, CeO_2–CeO_2, and NiO–CeO_2) formed in the NiO/CeO_2 NC sensor which can be modulated in the presence of targeted gas and fresh air. Among them, the junction formed at the interface of p-NiO and n-CeO_2 is the greatest contributor to the enhanced sensing performance of NiO/CeO_2 NC sensor than pure CeO_2 sensor. As discussed above, decoration of p-NiO on n-CeO_2 initiates the diffusion of majority charge carriers (holes in NiO side and electrons in CeO_2 side) to opposite sides until the equalization of their Fermi levels, which results in the development of an internal potential (built-in potential) at the junction. This built-in potential further reduces the conducting region of CeO_2 and helps in the enhanced sensing performance by the variation of its width during the adsorption and desorption of air and targeted gas. NiO/CeO_2 NC sensor possess electrons as majority carriers, which made it predominantly an n-type metal oxide sensor. In air atmosphere free electrons from NiO/CeO_2 NC sensor will be trapped by adsorbed oxygen molecules and form negatively charged ion species ($O_{(ads)}^{2-}$, $O_{2(ads)}^{-}$, $O_{(ads)}^{-}$, and $O_{2(ads)}^{2-}$). This trapping of electrons from the sensor material increases the width of the built-in potential as well as decreases the conducting region of CeO_2, which further increases the resistance of the sensor. In the presence of target isopropanol gas, trapped electrons will be released back to the sensor due to the reaction of isopropanol with adsorbed oxygen ions and decreases the width of the built-in potential and increases the volume of conducting region of CeO_2, which presumably causes to the drastical decrease in the sensor resistance. These huge resistance changes of the sensor in the presence of air and targeted isopropanol lead to the tremendous response of NiO/CeO_2 NC sensor than pure CeO_2 sensor. In addition to this built-in potential mechanism, surface adsorbed oxygen theory which is discussed for pure CeO_2 sensor is also applicable here. The whole process is schematically shown in Fig. 10(c)

Chemical sensitization with great catalytic activity of decorated p-NiO plays an important role in enhancing the sensor response.[49] The adsorption and desorption rates of the molecular oxygen and test gas will be greatly enhanced by the chemical sensitization of p-NiO on the surface of the sensor.

The catalytic activity of the NiO increases the reaction rate by decomposing of the test gas molecules to facilitate its oxidation on the surface of the sensor. Every individual gas which was tested in this experiment has its own physico-chemical properties like, bond dissociation energy, volatility, partial pressure *etc.* which affect the gas sensing performance greatly. The molecular interaction of targeted gas with adsorbed oxygen species, and its dissimilar molecular interactions on NiO/CeO_2 sensor surface significantly affect the sensing performance. The reactions occurred during the gas sensing test are discussed below. All the gases tested in the experiment were reducing in nature.

The exposure of NiO decorated CeO_2 sensor to isopropanol gas at room temperature reacts with the adsorbed oxygen and leads to the formation of CO_2 and H_2O along with the release of plenty of free electrons which reduces the sensor resistance. Isopropanol gas interacts with the adsorbed oxygen ($O_{2(ads)}^-$) as per the following reaction.

$$(CH_3)_2CHOH + 4O_{2(ads)}^- \rightarrow 3CO_2 + 3H_2O + H_2 + 4e^- \quad (3)$$

Finally, the highly porous nature, built-in potential developed at the interface of NiO and CeO_2, unique catalytic properties and chemical sensitization of NiO and respective physico-chemical properties of individual gas influenced the gas sensing performance of NiO and CeO_2 gas sensor and helped in the enhanced sensing behavior than pure CeO_2 sensors.

Conclusion

CeO_2 nanostructures were synthesized by using co-precipitation technique and NiO was decorated on the surface of CeO_2 by sol–gel process. Structural, morphological and compositional studies were carried out systematically. Perfect decoration of NiO on CeO_2 surface was confirmed from HRTEM analysis. SEM studies revealed the porous nature of the NiO/CeO_2 sensor surface. Pristine CeO_2 and NiO/CeO_2 sensors were subjected to their gas sensing studies under room conditions and observed enhanced gas sensing properties for NiO/CeO_2 sensor towards isopropanol. A highest response of ~1570 was observed for NiO/CeO_2 NCs based gas sensor which is nearly 11 times higher than the pure CeO_2 based gas sensor (~139) towards 100 ppm isopropanol at room temperature. Sharp response and recovery times (15 s/19 s) were obtained for NiO/CeO_2 sensor towards 100 ppm isopropanol at room temperature, and long-term stability also found from the studies.

Conflicts of interest

There are no conflicts to declare.

Acknowledgements

The authors thank the Head, Department of Physics, Osmania University, Hyderabad for providing necessary experimental facilities to carry out this work. The authors (NJB & JS) thankful to DST, New Delhi, India for providing financial assistance in the form of INSPIRE FELLOWSHIP during the research work. One of the authors (MVRR) thanks DST-SERB (File No.: EMR/2017/002651) for providing necessary financial support to carryout this work. A part of the reported work (characterization) was carried out at the NCPRE, IITB under PUMP which is sponsored by MNRE, Government of India. A part of the reported work (characterization) was carried out at the IITB under INUP which is sponsored by DeitY, MCIT, Government of India.

References

1 T. Montini, M. Melchionna, M. Monai and P. Fornasiero, *Chem. Rev.*, 2016, **116**, 5987–6041.
2 T. N. Ravishankar, T. Ramakrishnappa, G. Nagaraju and H. Rajanaika, *ChemistryOpen*, 2015, **4**, 146–154.
3 S. Rajeshkumar and P. Naik, *Biotechnol. Rep.*, 2018, **17**, 1–5.
4 S. Das, J. M. Dowding, K. E. Klump, J. F. McGinnis, W. Self and S. Seal, *Nanomedicine*, 2013, **8**, 1483–1508.
5 P. Tamizhdurai, S. Sakthinathan, S.-M. Chen, K. Shanthi, S. Sivasanker and P. Sangeetha, *Sci. Rep.*, 2017, **7**, 46372.
6 M. Sivakumar, M. Sakthivel and S.-M. Chen, *RSC Adv.*, 2016, **6**, 104227–104234.
7 S. Yan, X. Liang, H. Song, S. Ma and Y. Lu, *Ceram. Int.*, 2018, **44**, 358–363.
8 X. Yang, X. Hao, T. Liu, F. Liu, B. Wang, C. Ma, X. Liang, C. Yang, H. Zhu, J. Zheng, T. He and G. Lu, *Sens. Actuators, B*, 2018, **269**, 118–126.
9 J. Wang, Z. Li, S. Zhang, S. Yan, B. Cao, Z. Wang and Y. Fu, *Sens. Actuators, B*, 2018, **255**, 862–870.
10 S. M. A. Durrani, M. F. Al-Kuhaili, I. A. Bakhtiari and M. B. Haider, *Sensors*, 2012, **12**, 2598–2609.
11 A. Wahid, A. M. Asiri and M. M. Rahman, *Environ. Nanotechnol. Monit. Manage.*, 2018, **10**, 314–321.
12 Z. Zhao, X. Liu, X. Xing, Y. Lu, Y. Sun, X. Ou, X. Su, J. Jiang, Y. Yang, J. Chen, B. Shen and Y. He, *PLoS One*, 2016, **11**, e0162762.
13 H. M. Burlage and D. B. Hawkins, *J. Am. Pharm. Assoc.*, 1946, **35**, 379–384.
14 O. Desy, D. Carignan, M. Caruso and P. O. de Campos-Lima, *J. Immunol.*, 2008, **181**, 2348–2355.
15 D. Hu, B. Han, S. Deng, Z. Feng, Y. Wang, J. Popovic, M. Nuskol, Y. Wang and I. Djerdj, *J. Phys. Chem. C*, 2014, **118**, 9832–9840.
16 Y.-L. Wu, Q. Luan, S.-J. Chang, Z. Jiao, W. Y. Weng, Y.-H. Lin and C. L. Hsu, *IEEE Sens. J.*, 2014, **14**, 401–405.
17 X. Cai, D. Hu, S. Deng, B. Han, Y. Wang, J. Wu and Y. Wang, *Sens. Actuators, B*, 2014, **198**, 402–410.
18 B. Zhang, W. Fu, X. Meng, R. A, P. Su and H. Yang, *Appl. Surf. Sci.*, 2018, **456**, 586–593.
19 M. Poloju, N. Jayababu, E. Manikandan and M. V. Ramana Reddy, *J. Mater. Chem. C*, 2017, **5**, 2662–2668.
20 C. Fan, G. Liu, Y. Zhang and M. Wang, *Mater. Lett.*, 2017, **209**, 8–10.
21 S.-H. Li, Z. Chu, F.-F. Meng, T. Luo, X.-Y. Hu, S.-Z. Huang and Z. Jin, *J. Alloys Compd.*, 2016, **688**, 712–717.
22 D. Hu, B. Han, R. Han, S. Deng, Y. Wang, Q. Li and Y. Wang, *New J. Chem.*, 2014, **38**, 2443.

23 J. Zhang, X. Liu, G. Neri and N. Pinna, *Adv. Mater.*, 2016, **28**, 795–831.
24 S. Park, G.-J. Sun, C. Jin, H. W. Kim, S. Lee and C. Lee, *ACS Appl. Mater. Interfaces*, 2016, **8**, 2805–2811.
25 X. Deng, L. Zhang, J. Guo, Q. Chen and J. Ma, *Mater. Res. Bull.*, 2017, **90**, 170–174.
26 K. Fan, J. Guo, L. Cha, Q. Chen and J. Ma, *J. Alloys Compd.*, 2017, **698**, 336–340.
27 J. Ma, L. Mei, Y. Chen, Q. Li, T. Wang, Z. Xu, X. Duan and W. Zheng, *Nanoscale*, 2013, **5**, 895–898.
28 M. Bao, Y. Chen, F. Li, J. Ma, T. Lv, Y. Tang, L. Chen, Z. Xu and T. Wang, *Nanoscale*, 2014, **6**, 4063.
29 J. Pang, R. G. Mendes, A. Bachmatiuk, L. Zhao, H. Q. Ta, T. Gemming, H. Liu, Z. Liu and M. H. Rummeli, *Chem. Soc. Rev.*, 2019, **48**, 72–133.
30 J. Pang, A. Bachmatiuk, Y. Yin, B. Trzebicka, L. Zhao, L. Fu, R. G. Mendes, T. Gemming, Z. Liu and M. H. Rummeli, *Adv. Energy Mater.*, 2018, **8**, 1702093.
31 J. Pang, R. G. Mendes, P. S. Wrobel, M. D. Wlodarski, H. Q. Ta, L. Zhao, L. Giebeler, B. Trzebicka, T. Gemming, L. Fu, Z. Liu, J. Eckert, A. Bachmatiuk and M. H. Rümmeli, *ACS Nano*, 2017, **11**, 1946–1956.
32 F. Shu, M. Wang, J. Pang and P. Yu, *Front. Chem. Sci. Eng.*, 2018, DOI: 10.1007/s11705-018-1754-3.
33 K. Olszowska, J. Pang, P. S. Wrobel, L. Zhao, H. Q. Ta, Z. Liu, B. Trzebicka, A. Bachmatiuk and M. H. Rummeli, *Synth. Met.*, 2017, **234**, 53–85.
34 K. Wang, J. Pang, L. Li, S. Zhou, Y. Li and T. Zhang, *Front. Chem. Sci. Eng.*, 2018, **12**, 376–382.
35 R. G. Mendes, J. Pang, A. Bachmatiuk, H. Q. Ta, L. Zhao, T. Gemming, L. Fu, Z. Liu and M. H. Rümmeli, *ACS Nano*, 2019, **13**, 978–995.
36 G. S. Martynková, F. Becerik, D. Plachá, J. Pang, H. Akbulut, A. Bachmatiuk and M. H. Rummeli, *J. Nanosci. Nanotechnol.*, 2019, **19**, 2770–2774.
37 J. Hu, Y. Sun, Y. Xue, M. Zhang, P. Li, K. Lian, S. Zhuiykov, W. Zhang and Y. Chen, *Sens. Actuators, B*, 2018, **257**, 124–135.
38 M. Li, W. Ren, R. Wu and M. Zhang, *Sensors*, 2017, **17**, 1577.
39 J.-H. Kim, J.-H. Lee, A. Mirzaei, H. W. Kim and S. S. Kim, *Sens. Actuators, B*, 2018, **258**, 204–214.
40 M. ul Haq, Z. Wen, Z. Zhang, S. Khan, Z. Lou, Z. Ye and L. Zhu, *Sci. Rep.*, 2018, **8**, 1705.
41 H. Gao, L. Zhao, L. Wang, P. Sun, H. Lu, F. Liu, X. Chuai and G. Lu, *Sens. Actuators, B*, 2018, **255**, 3505–3515.
42 J. P. Holgado, R. Alvarez and G. Munuera, *Appl. Surf. Sci.*, 2000, **161**, 301–315.
43 A. Trinchi, *Sens. Actuators, B*, 2003, **95**, 145–150.
44 L. Liao, H. X. Mai, Q. Yuan, H. B. Lu, J. C. Li, C. Liu, C. H. Yan, Z. X. Shen and T. Yu, *J. Phys. Chem. C*, 2008, **112**, 9061–9065.
45 V. K. Tomer and S. Duhan, *J. Mater. Chem. A*, 2016, **4**, 1033–1043.
46 X. Lai, G. Shen, P. Xue, B. Yan, H. Wang, P. Li, W. Xia and J. Fang, *Nanoscale*, 2015, **7**, 4005–4012.
47 A. Dey, *Mater. Sci. Eng., B*, 2018, **229**, 206–217.
48 M. Poloju, N. Jayababu and M. V. Ramana Reddy, *Mater. Sci. Eng., B*, 2018, **227**, 61–67.
49 Z. Qu, Y. Fu, B. Yu, P. Deng, L. Xing and X. Xue, *Sens. Actuators, B*, 2016, **222**, 78–86.